SANDIA REPORT

SAND2015-8803
Unlimited Release
Printed October 2015

Albedo and Diffuse POA Measurements to Evaluate Transposition Model Uncertainty

Matthew Samuel Lave

Prepared by
Sandia National Laboratories
Albuquerque, New Mexico 87185 and Livermore, California 94550

Sandia National Laboratories is a multi-program laboratory managed and operated by Sandia Corporation, a wholly owned subsidiary of Lockheed Martin Corporation, for the U.S. Department of Energy's National Nuclear Security Administration under contract DE-AC04-94AL85000.

Approved for public release; further dissemination unlimited.



Sandia National Laboratories

Issued by Sandia National Laboratories, operated for the United States Department of Energy by Sandia Corporation.

NOTICE: This report was prepared as an account of work sponsored by an agency of the United States Government. Neither the United States Government, nor any agency thereof, nor any of their employees, nor any of their contractors, subcontractors, or their employees, make any warranty, express or implied, or assume any legal liability or responsibility for the accuracy, completeness, or usefulness of any information, apparatus, product, or process disclosed, or represent that its use would not infringe privately owned rights. Reference herein to any specific commercial product, process, or service by trade name, trademark, manufacturer, or otherwise, does not necessarily constitute or imply its endorsement, recommendation, or favoring by the United States Government, any agency thereof, or any of their contractors or subcontractors. The views and opinions expressed herein do not necessarily state or reflect those of the United States Government, any agency thereof, or any of their contractors.

Printed in the United States of America. This report has been reproduced directly from the best available copy.

Available to DOE and DOE contractors from
U.S. Department of Energy
Office of Scientific and Technical Information
P.O. Box 62
Oak Ridge, TN 37831

Telephone: (865) 576-8401
Facsimile: (865) 576-5728
E-Mail: reports@osti.gov
Online ordering: http://www.osti.gov/scitech

Available to the public from
U.S. Department of Commerce
National Technical Information Service
5301 Shawnee Rd
Alexandria, VA 22312

Telephone: (800) 553-6847
Facsimile: (703) 605-6900
E-Mail: orders@ntis.gov
Online order: http://www.ntis.gov/search



SAND2015-8803
Unlimited Release
Printed October 2015

Albedo and Diffuse POA Measurements to Evaluate Transposition Model Uncertainty

Matthew Samuel Lave
Photovoltaic and Distributed Systems Integration
Sandia National Laboratories
P.O. Box 969, MS-9052
Livermore, California 94551-0969

Abstract

Albedo and diffuse plane of array (DPOA) measurements are used in addition to standard global horizontal irradiance (GHI), direct normal irradiance (DNI), diffuse horizontal irradiance (DNI), and plane of array irradiance (POA) measurements to determine the impact of albedo on transposition model performance. Albedo measurements averaged 0.214. Daily albedo values ranged from 0.148 to 0.236 and were found to be correlated to daily relative humidity. DPOA measurements were compared to calculated DPOA values (from POA and DNI), and helped identify a suspected deviation from due south in the azimuth of the POA measurement.

Since the measured albedo average was close to the typical fixed $albedo = 0.2$ assumption, little difference was seen between using measured and fixed albedo (~0.15% differences in mean bias difference (MBD) and root mean squared difference (RMSD)). However, evaluation of transposition models at other fixed albedos showed an albedo change of 0.1 is found to increase total modeled insolation by approximately 1%. Thus, for locations with different ground surfaces (e.g., persistent snow cover of black surfaces), the impact of using measured albedo instead of the fixed $albedo = 0.2$ assumption may be greater.

Measurement deviations resulted in up to 2% changes in MBD and RMSD when switching between interrelated measurements (e.g., GHI and DHI as inputs to transposition models versus DNI and DHI as inputs). Variation among transposition models was also up to 2% MBD and RMSD. Thus, for this data set, measurement deviation and transposition model selection are found to have more impact than using measured albedo instead fixed albedo.

CONTENTS

1. Introduction 7

2. Irradiance Measurements 9
   2.1. Measurement Descriptions 9
   2.2. Data Availability and Resolution 9
   2.3. Identified Clear Days 11
   2.4. Measurement Deviation 11

3. Transposition Models Evaluated 13
   3.1. Isotropic Transposition Model ("isotropic") 13
   3.2. Sandia Transposition Model ("King") 14
   3.3. Hay and Davies Transposition Model ("Hay/Davies") 14
   3.4. Perez Transposition Model ("Perez") 14

4. Albedo and DPOA Measurement Analysis 17
   4.1. Albedo 17
   4.2. Diffuse Plane of Array (DPOA) 23

5. Effect of Measured Albedo on POA modeling 29
   5.1. Modeled versus Measured over Period of Record 29
   5.2. Time of Day Dependence 30
   5.3. Effect of Assumed Albedo 31
   5.4. Hourly Analysis 33

6. Conclusions 35

References 37

Distribution 39

FIGURES

Figure 1: Two CMP-11 pyranometers, one mounted up to capture GHI, the other mounted down to capture ground reflected irradiance (GRI). Combined, these instruments allow for albedo measurements. 10

Figure 2: CMP-11 pyranometer, tilted to latitude tilt (35°) and with a shadow band, allowing for measurements of diffuse plane of array irradiance (DPOA). 10

Figure 3: [Top] GHI measurements from the weather station (solid lines) and the albedometer (dashed lines) on the five clear days. [Bottom] Difference (weather station GHI minus albedometer GHI) for each day. 12

Figure 4: [Top] GHI (solid lines) and GRI (dashed lines) on 5 clear days. [Bottom] Calculated albedo (GRI/GHI) for the same days. 17

Figure 5: GRI vs. GHI for all days (black dots), and for the 5 clear days (colored dots), with albedo contours shown as red dashed lines. 18

Figure 6: Mean daily albedo for times when the solar elevation angle was greater than 10° (to eliminate morning and evening effects). 19

Figure 7: [Top] GHI (solid lines) and GRI (dashed lines) on the 3 days with lowest daily averaged albedos. [Bottom] Calculated albedo (GRI/GHI) for the same days..... 20
Figure 8: Daytime average albedo plotted as a function of daytime averaged relative humidity, with colors indicating daytime average temperature. 21
Figure 9: Spectral plots for [top] a clear day (April 19th) and [bottom] a partly cloudy day with low daily average albedo (May 16th). Left plots show absolute intensity, right plots show normalized intensity. The average spectrum for April 19th is included as a dashed black line on the May 16th plots for reference. 22
Figure 10: Timeseries of DPOA measurements. The times highlighted in red were filtered out due to the shadowband being misaligned. 23
Figure 11: [Top] POA and DPOA on the 5 clear days. [Bottom] Angle of incidence (AOI) for the 35° tilted POA measurement on the 5 clear days. 24
Figure 12: Calculated DPOA (using Equation 12) plotted against measured DPOA. Mean bias difference (MBD), mean absolute difference (MAD), and root mean squared difference (RMSD) statistics describing the difference $DPOA_{calc}$ minus DPOA are shown in the top left. 25
Figure 13: [Top] Measured DPOA and calculated DPOA (using Equation 12). [Bottom] Difference (calculated DPOA minus measured DPOA). 26
Figure 14: [Top Left] Difference (morning minus afternoon) in POA irradiance, plotted as a function of angle of incidence at a 30° tilt, due south azimuth. [Bottom Left] Same as top left, but for DNI. [Right Plots] Same as top left, but assuming varying azimuths..... 26
Figure 15: Negative (red) values of $DPOA_{calc}$ as a function of solar azimuth and elevation. The values in the blue box were filtered out of the analysis due to likely shading of the POA sensor. 27
Figure 16: POA, DNI*cos(AOI), and $DPOA_{calc}$ for clear day June 14th. The dashed portions around 06:30 show the effect of filtering out the shaded POA periods seen in Figure 15. 28
Figure 17: [Top] Mean bias difference and [Bottom] root mean squared difference for combinations of transposition inputs and POA measurements (colors) and for four transposition models (x-axis)..... 30
Figure 18: Mean error for each time of day. The different plots [top left, top right, bottom left, bottom right] show the different transposition models, and the various lines (different colors) show the various transposition inputs and POA measurements. 31
Figure 19: [Top] Mean bias difference and [Bottom] root mean squared difference for different fixed albedo assumptions (colored lines) using four transposition models (x-axis)..... 32
Figure 20: Same as Figure 17, but computed using hourly data. 33
Figure 21: Same as Figure 18, but computed using hourly data. 34

TABLES

Table I: Temperature and relative humidity (RH) dependent statistics of daytime albedo. 21

1. INTRODUCTION

PV performance models which model the power production of PV arrays require irradiance incident on the array's plane as an input. However, plane of array (POA) irradiance at the specific plane of the PV modules is often not measured, and instead POA irradiance is modeled from more common measurements of global horizontal irradiance (GHI), diffuse horizontal irradiance (DHI), and direct normal irradiance (DNI). When only GHI measurements are available, decomposition models (e.g., Erbs [1], DIRINT [2], etc.) can be used to approximate DNI and DHI. If either DNI or DHI is measured along with GHI (or if DNI and DHI are both measured without GHI), then the decomposition models can be skipped and instead only a transposition model is used to approximate the POA irradiance.

Transposition models compute the POA irradiance in three components: direct irradiance incident on the plane, sky diffuse irradiance, and ground reflected irradiance. Previous evaluations (e.g., [3-6]) have evaluated the performance of transposition models at matching POA irradiance measurements. In most cases, and albedo of 0.2 was assumed to be representative of the surrounding ground surface. Occasionally, albedo measurements were used, but little focus was given to analyzing the variation of albedo by hour or by day.

In this work, we use albedo and diffuse plane of array (DPOA) measurements to explore the variation of albedo and the impact that albedo can have on transposition model performance. Special attention is given to interrelated measurements such as GHI, DNI, and DHI, any two of which can be used to create the third. Similarly, any two of DNI, POA, and DPOA can be used to create the third. Various combinations of these interrelated measurements are used to run transposition models to show the impact of measurement uncertainties comparted to the impact of changing albedo.

We describe the weather station and albedometer measurements used for this study, including data resolution and availability, in Section 2. The transposition models evaluated are explained in detail in Section 3. Section 4 analyzes the albedo and DPOA measurements, including exploring low albedo days and their relation to high relative humidity and evaluating discrepancies between the DPOA measurements and the related DNI and POA measurements. Transposition model results when using measured albedo versus fixed albedo are compared in Section 5. The conclusions of our study are presented in Section 6.

2. IRRADIANCE MEASUREMENTS

2.1. Measurement Descriptions

Irradiance measurements available for this work include standard global horizontal irradiance (GHI), diffuse horizontal irradiance (DHI), direct normal irradiance (DNI), and global plane of array irradiance (POA) on a surface tilted 35° and a due south azimuth. GHI is measured with a Kipp and Zonen CMP21, DHI is measured with an Eppley precision spectral pyranometer (PSP) with shade disk, DNI is measured with a temperature corrected Kipp and Zonen CHP1, and POA is measured with an incident angle corrected Eppley PSP.

In addition to these typical measurements, two atypical measurements – ground reflected irradiance (GRI) and diffuse plane of array (DPOA) – were also collected for this study. GRI was captured using a CMP-11 pyranometer pointed at the ground, and was co-located with a sky-facing CMP-11 measuring GHI, as shown in Figure 1, forming an albedometer. Following the convention of nearly all irradiance translation studies which have assumed that the ground reflection process is ideally isotropic [3], ground albedo (ρ) can be calculated as:

$$\rho = \frac{GRI}{GHI} \tag{1}$$

POA was measured using a CMP-11 tilted 35° and a shadowband to block the direct irradiance, as shown in Figure 2. The shadowband was manually adjusted every few days to block direct sunlight. Measurements are adjusted to account for the fraction of the sky dome obscured by the shadowband using the correction described in the Kipp and Zonen CM121 shadow ring manual [7].

All measurements were taken at Sandia National Laboratories' Photovoltaic and Systems Integration Laboratory (PSEL) in Albuquerque, NM. The GRI and DPOA measurements were collected in open space approximately 75 meters west of the traditional irradiance measurements which are part of an outdoor weather station. GHI was collected at both locations: as part of the instrument table setup and also co-located with the GRI measurement. Comparison of the two GHI measurements ensured time-syncing of all measurements.

2.2. Data Availability and Resolution

GRI and DPOA measurements were available from March 24th through September 1st, 2015. GHI, DHI, DNI, and POA measurements have a much longer period or record (more than 10 years), but analysis was limited to these dates to show the value of GRI and DPOA measurements. Additionally, POA measurements on April 2nd, July 1st, and from August 27-31st were errant and so were removed from the analysis. DHI measurements on March 26th and April 2nd were roughly equal to GHI during clear periods, indicating a likely misalignment of the shading disk used for DHI measurements, so were removed from the analysis. DNI measurements on March 26th, May 22nd, and August 29th were zero when other instruments indicated there should have been some amount of DNI, so these measurements were removed.

Data was recorded at 15-second resolution for the GRI and DPOA measurements and at approximately 3-second resolution for all other measurements. However, due to the slow response time of the instruments and to ensure proper time syncing between measurements, all

data are averaged over time and the analysis is performed at 1-minute or longer time intervals. If not stated otherwise, plots were created using 1-minute averaged data.



Figure 1: Two CMP-11 pyranometers, one mounted up to capture GHI, the other mounted down to capture ground reflected irradiance (GRI). Combined, these instruments allow for albedo measurements.



Figure 2: CMP-11 pyranometer, tilted to latitude tilt (35°) and with a shadow band, allowing for measurements of diffuse plane of array irradiance (DPOA).

2.3. Identified Clear Days

Based on visual inspection of the available data, five days were selected as fully clear days. These five days –March 27th, March 28th, April 29th, June 14th, and August 19th – are often shown separately in the analysis that follows to understand albedo and GPOA during clear conditions.

2.4. Measurement Deviation

Comparison of the duplicate GHI measurements at the weather station and albedometer give an indication of GHI measurement deviation. Figure 3 shows the weather station measured GHI and the GHI measured at the albedometer on the five clear days. Coarse visual inspection shows good agreement, that is, the data is time synched, both locations measured a clear-sky profile, etc. However, closer inspection shows that there was a small difference in the measurements on each clear day morning (approximately 6:30 to 11:00). During these times, the weather station GHI was up to 10 Wm^{-2} less than the albedometer GHI. Possible causes of this discrepancy include slightly different fields of view in the morning (the weather station GHI measurement is on an instrument bench approximately 8 meters off the ground, while the albedometer measurement is mounted only about 1 meter off the ground) and slight (<1°) offsets in mounting orientation which would affect the amount of direct irradiance incident on each sensor. Since an exact cause of this discrepancy could not be identified, we proceed with our analysis with the note that we have disagreement among GHI instruments of up to 10 Wm^{-2}. There are likely additional unobserved measurement uncertainties.

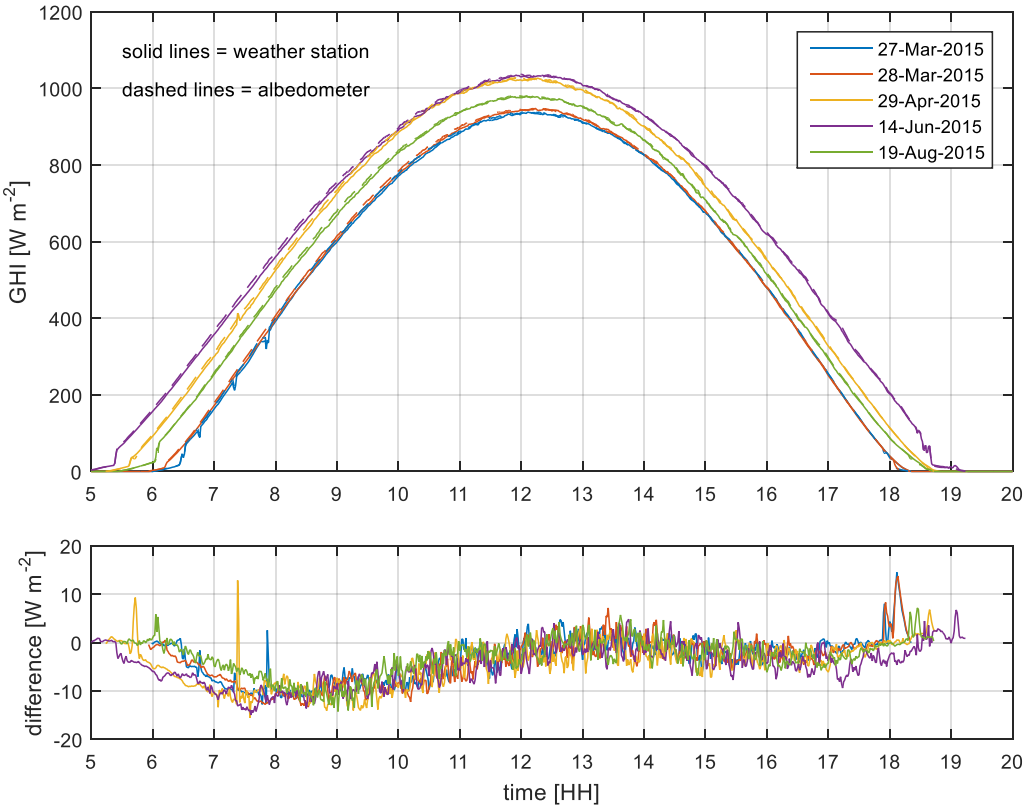


Figure 3: [Top] GHI measurements from the weather station (solid lines) and the albedometer (dashed lines) on the five clear days. [Bottom] Difference (weather station GHI minus albedometer GHI) for each day.

3. TRANSPOSITION MODELS EVALUATED

Transposition models estimate POA irradiance, i.e., the irradiance incident on a tilted plane. On the horizontal surface, there are two components of solar radiation: direct and diffuse. On an inclined surface, there are three: direct, sky diffuse, and ground reflected diffuse. To model the POA irradiance on an inclined surface, the three components are summed together:

$$\mathrm{POA} = \mathrm{POA}_{\mathrm{direct}} + \mathrm{POA}_{\mathrm{diff,\ sky}} + \mathrm{POA}_{\mathrm{diff,\ refl}} \tag{2}$$

The direct irradiance on the inclined surface (POA_{direct}) is a function of the DNI and the angle of incidence AOI of the direct beam on the tilted surface:

$$\mathrm{POA}_{\mathrm{direct}} = \mathrm{DNI} \times \cos\left(\mathrm{AOI}\right) \tag{3}$$

The AOI is a function of the solar altitude and solar azimuth as well as the inclined surface's tilt from horizontal (*SurfTilt*) and azimuth orientation (*SurfAz*):

$$\mathrm{AOI} = \cos^{-1}\left[\sin\left(\mathit{SunEl}\right)\cos\left(\mathit{SurfTilt}\right) + \sin\left(\mathit{SurfTilt}\right)\cos\left(\mathit{SunEl}\right)\mathrm{cosd}\left(\mathit{SunAz} - \mathit{SurfAz}\right)\right] \tag{4}$$

Although ground reflected irradiance ($\mathrm{POA}_{\mathrm{diffuse,\ refl}}$) cannot be directly calculated, nearly all authors with the noted exception of the Sandia model by King [8] have used the same model [5]. This ground diffuse model assumes that GHI is reflected isotropically from each point on the ground. $\mathrm{POA}_{\mathrm{diff,refl}}$ is then estimated by multiplying the GHI by the ground albedo (*albedo*) by the fraction of the sky dome in front of the tilted surface to determine $\mathrm{POA}_{\mathrm{diff,\ refl}}$:

$$\mathrm{POA}_{\mathrm{diff,\ refl}} = \mathrm{GHI} \times \mathit{albedo} \times \frac{1 - \cos\left(\mathit{SurfTilt}\right)}{2} \tag{5}$$

While the ground albedo can vary due to seasonal vegetation changes and snow cover, when albedo measurements are not available, it is typical to assign $albedo = 0.2$.

Consequently, transposition models vary primarily in the treatment of the sky diffuse irradiance $\mathrm{POA}_{\mathrm{diff,\ sky}}$ on the inclined surface. The earliest, and simplest, transposition model is the isotropic model, which assumes that diffuse irradiance is isotropic across the hemispherical sky. Liu and Jordan [9] is often cited as the first publication of this model. As observations showed that diffuse irradiance is not isotropic (e.g., [10]), model complexity has increased to better describe the observed anisotropy, and it's variation with sun position and atmospheric conditions.

In our analysis we consider the four transposition models described in the following sections since they are in popular and common use. Full model descriptions are given in the following sections. Many others transposition models are available; WŁOdarczyk and Nowak [6] provide a summary and comparison of 14 transposition models.

3.1. Isotropic Transposition Model ("isotropic")

The eponymous isotropic model [11] assumes that diffuse irradiance is uniform across the hemisphere and calculates diffuse irradiance on the tilted plane as

$$\mathrm{POA}_{\mathrm{diff,\ sky}} = \mathrm{DHI} \times \frac{1 + \cos(\mathit{SurfTilt})}{2} \tag{6}$$

where the fraction simply expresses the fraction of the hemispheric sky dome that is in front of the inclined surface.

3.2. Sandia Transposition Model ("King")

The Sandia transposition model by King [8] is an empirical formula to predict diffuse irradiance on an inclined plane, using measured DHI and GHI as predictors. The model was developed using data from Albuquerque, NM. Diffuse irradiance (both sky and ground reflected) on a tilted plane was estimated as the difference between POA irradiance and direct irradiance as measured by a pyrheliometer and translated to the plane-of-array by Equation (3). The model uses the isotropic transposition model for sky diffuse (Equation (6)) combined with the following empirical expression for ground reflected diffuse irradiance:

$$\mathrm{POA}_{\mathrm{diff,\ refl}} = \mathrm{GHI} \times \left(0.012 \times \mathit{SunZen} - 0.04\right) \times \frac{1-\cos(\mathit{SurfTilt})}{2} \tag{7}$$

where *SunZen* is the solar zenith angle in degrees, to obtain total diffuse irradiance on a tilted plane as

$$\begin{aligned} \mathrm{POA}_{\mathrm{diff}} &= \mathrm{POA}_{\mathrm{diff,\ sky}} + \mathrm{POA}_{\mathrm{diff,\ refl}} \\ &= \mathrm{DHI} \times \frac{1+\cos(\mathit{SurfTilt})}{2} + \mathrm{GHI} \times \left(0.012 \times \mathit{SunZen} - 0.04\right) \times \frac{1-\cos(\mathit{SurfTilt})}{2} \end{aligned} \tag{8}$$

Essentially, the Sandia transposition model replaces the constant albedo *albedo* in Equation (5) with the empirical expression $\mathit{albedo} = 0.012 \times \mathit{SunZen} - 0.04$. Care should be taken when applying this model generally, because the data underlying the empirical expression for albedo represent conditions at the Photovoltaic System Evaluation Laboratory (PSEL), which is part of Sandia National Laboratories in Albuquerque, NM, where little to no snowfall is present and the southward view comprises buildings and parking lots.

3.3. Hay and Davies Transposition Model ("Hay/Davies")

The Hay and Davies [12] model separates sky diffuse irradiance into two components, circumsolar and rest-of-sky. Circumsolar diffuse irradiance on the tilted plane is considered in the same manner as direct irradiance, whereas rest-of-sky diffuse irradiance is considered to be uniform over the hemisphere. The fraction of sky diffuse irradiance that is circumsolar diffuse irradiance is defined using an anisotropy index A:

$$A = \frac{\mathrm{DNI}}{\mathit{HExtra}} \tag{9}$$

where *HExtra* is extraterrestrial normal irradiance. Using the index A the sky diffuse irradiance on the tilted plane is calculated as:

$$\mathrm{POA}_{\mathrm{diff,\ sky}} = \mathrm{DHI} \times \left[A \times \frac{\cos \mathrm{AOI}}{\cos(\mathit{SunZen})} + \left(1 - A\right) \frac{1+\cos(\mathit{SurfTilt})}{2} \right]. \tag{10}$$

3.4. Perez Transposition Model ("Perez")

The Perez [13] transposition model, separates sky diffuse irradiance into three components: circumsolar; near-horizon; and rest-of-sky. The sky diffuse irradiance on the tilted plane is estimated by

$$\mathrm{POA}_{\mathrm{diff,\,sky}} = \mathrm{DHI} \times \left[F_1 \frac{a}{b} + F_2 \sin(SurfTilt) + \left(1 - F_1\right) \frac{1 + \cos(SurfTilt)}{2} \right] \tag{11}$$

where the three terms in the sum are the circumsolar, horizon brightening, and rest-of-sky diffuse components, in that order. The terms a and b involve AOI and the solar zenith angle, while the coefficients F_1 and F_2 result from a set of complicated empirical expressions involving DHI, DNI, extraterrestrial normal irradiance, solar zenith angle, and air mass, fitted to a large data set. The equations are summarized in [5] whereas empirical coefficients are given in [13].

4. ALBEDO AND DPOA MEASUREMENT ANALYSIS

4.1. Albedo

Albedo values were calculated using Equation 1. We first examined the albedos on clear days when cloud-reflections are not present. Clear days should best follow the isotropic ground reflection assumption, although variance in the ground surrounding the sensors may still lead to slight anisotropic effects. Figure 4 shows GHI, GRI, and calculated albedo for the 5 clear days.

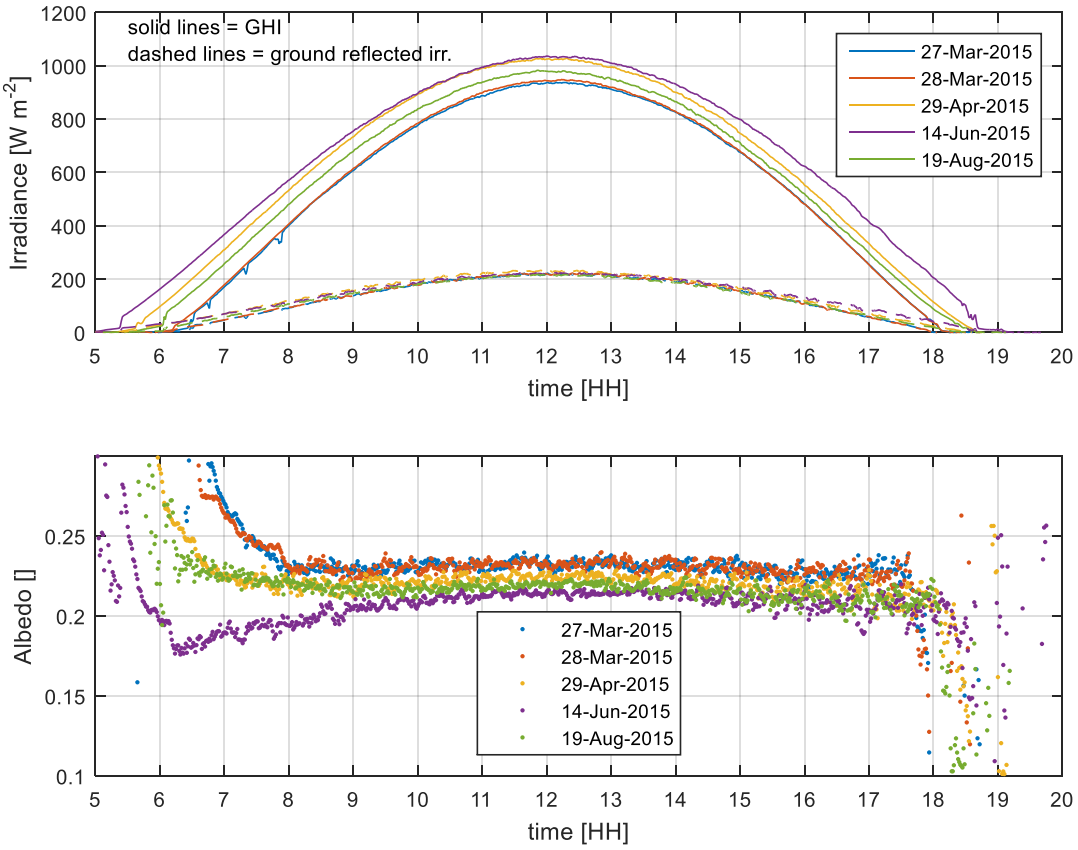


Figure 4: [Top] GHI (solid lines) and GRI (dashed lines) on 5 clear days. [Bottom] Calculated albedo (GRI/GHI) for the same days.

During the middle of the day (~09:00-17:00), the albedo values on the clear days are fairly consistent. Albedo values were almost always between 0.2 and 0.25 during these hours, although there is slight variation from day-to-day. Generally, there are high albedo values seen in the mornings (higher than 0.25) and low albedo values seen in the evenings (lower than 0.2). These extreme values may be caused horizon shading in the morning and near field shading in the evening.

Figure 5 shows GRI vs. GHI for all days, where albedo can be read as diagonal contours. The five clear days shown in Figure 4 are highlighted in Figure 5 to reveal how the clear day albedos compare to the rest of the days. During mid and high irradiance periods (i.e., GHI > 300 Wm^{-2}), albedo values were almost always (99.9% of minutes) between 0.15 and 0.25. During high irradiance periods (GHI > 800 Wm^{-2}), the range of albedo values became slightly narrower and shifted slightly to larger albedos: nearly all (99.7% of minutes) albedo values were between 0.175 and 0.25. The overall average albedo for all GHI values when the solar elevation angle was greater than 10° was 0.214.

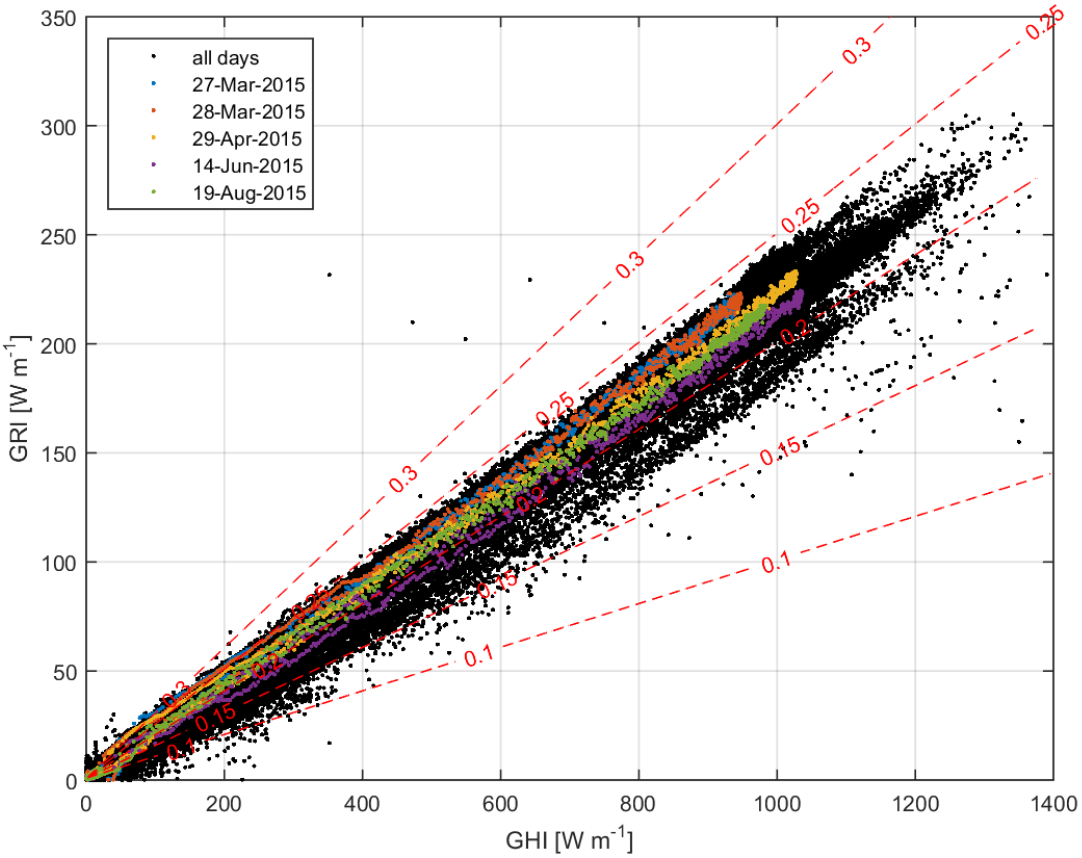


Figure 5: GRI vs. GHI for all days (black dots), and for the 5 clear days (colored dots), with albedo contours shown as red dashed lines.

To examine albedo by day, Figure 6 shows the daily albedo, averaged over all times during each day when the solar elevation angle was greater than 10°. This solar elevation angle filter was chosen to eliminate times when the directional response errors of the CMP11 sensors are expected to be large [14]. Daily albedo values are generally between 0.18 and 0.24, with notable exceptions on April 26th, May 5th, and May 16th, when daily averaged albedos were all less than 0.16. The average daily albedo was 0.214, consistent with the average albedo found for the minute albedo values.

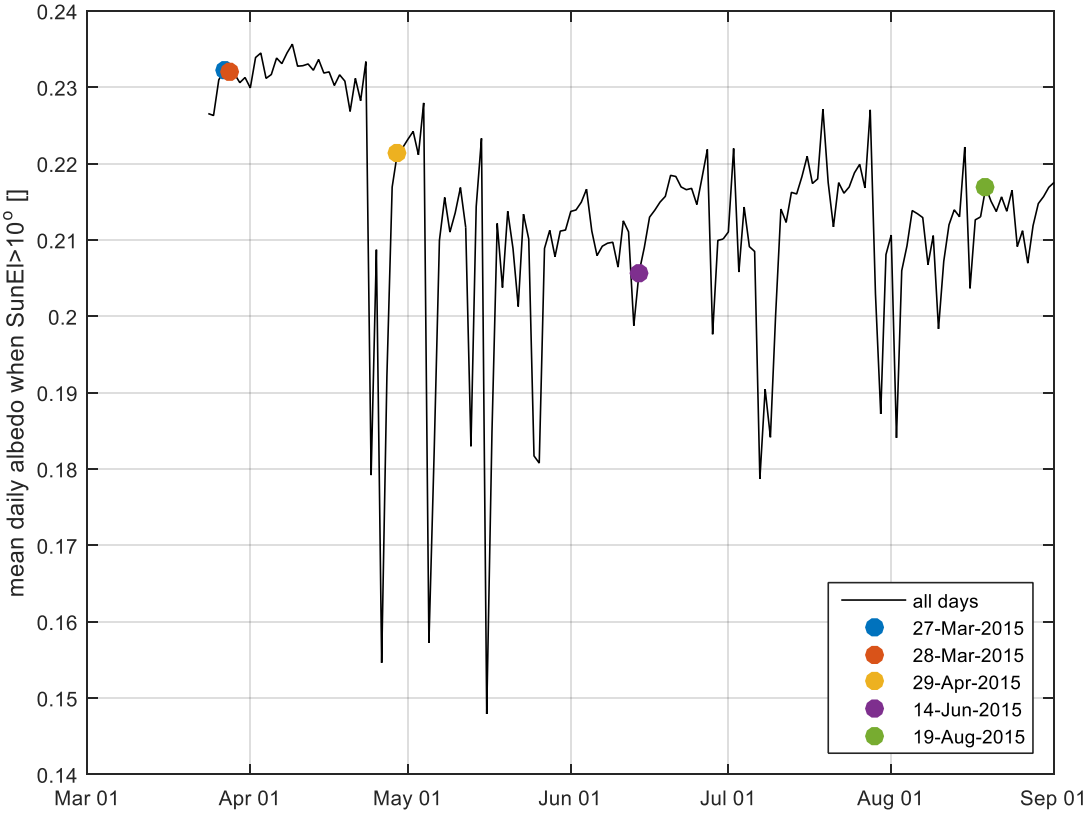


Figure 6: Mean daily albedo for times when the solar elevation angle was greater than 10° (to eliminate morning and evening effects).

Figure 7 examines the 3 days with lowest daily average albedos. The GHI profiles show that these were all partly clouds days. Albedo values were small during all midday periods, but there are occasional periods of especially small albedo (e.g., around 11:30 on May 16th).

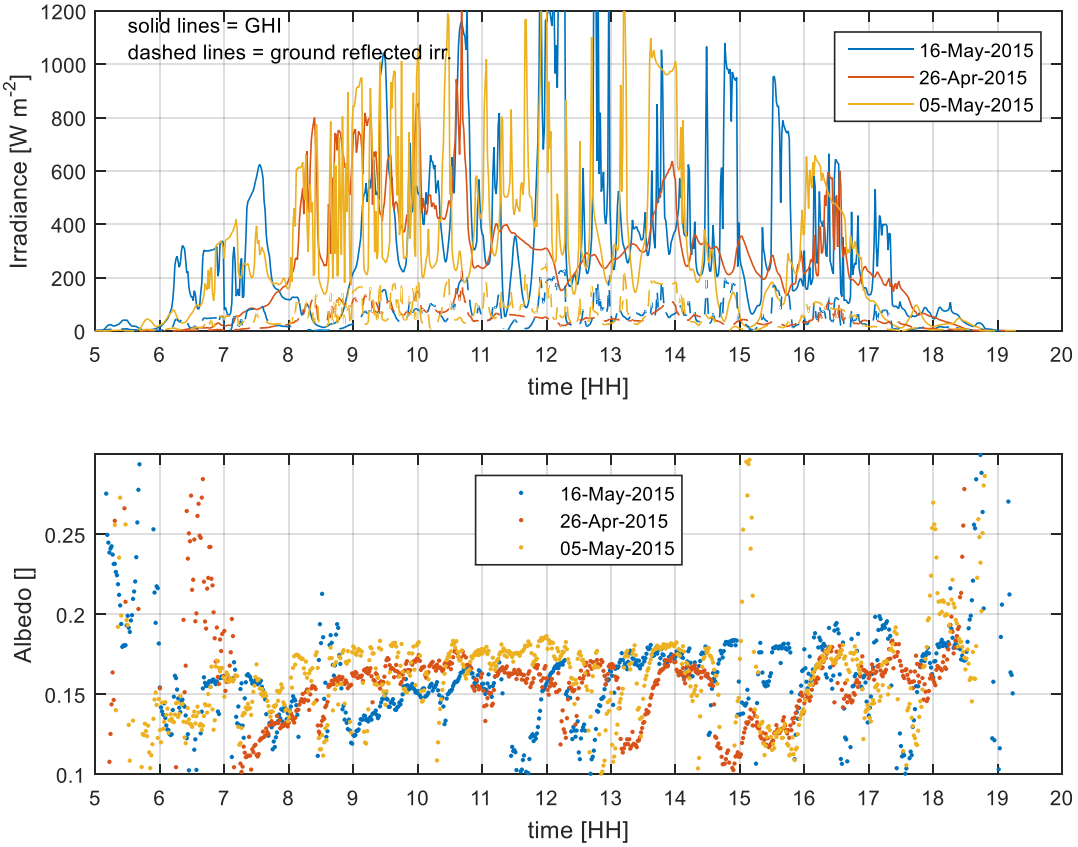


Figure 7: [Top] GHI (solid lines) and GRI (dashed lines) on the 3 days with lowest daily averaged albedos. [Bottom] Calculated albedo (GRI/GHI) for the same days.

The three days shown in Figure 7, which were the days with the lowest albedos, were also found to have some of the lowest daily averaged relative humidity values. Figure 8 is a scatter plot of the daily average albedo against the daily average relative humidity, where dot colors indicate daily average temperature. All daily average values were calculated from all minutes when the solar altitude angle was greater than 10°, just as done in Figure 6. Two trends are evident in Figure 8: (1) that daily albedo and daily relative humidity are negatively correlated – as relative humidity increases, albedo generally decrease; and (2) when temperature is above 25°C, the albedos average 0.2133 with small deviation, regardless of the humidity (although relative humidity exceeding 50% is not observed in our data for temperature above 25°C). These trends are summarized in Table I, which constitutes an empirical model for albedo at this Albuquerque location.

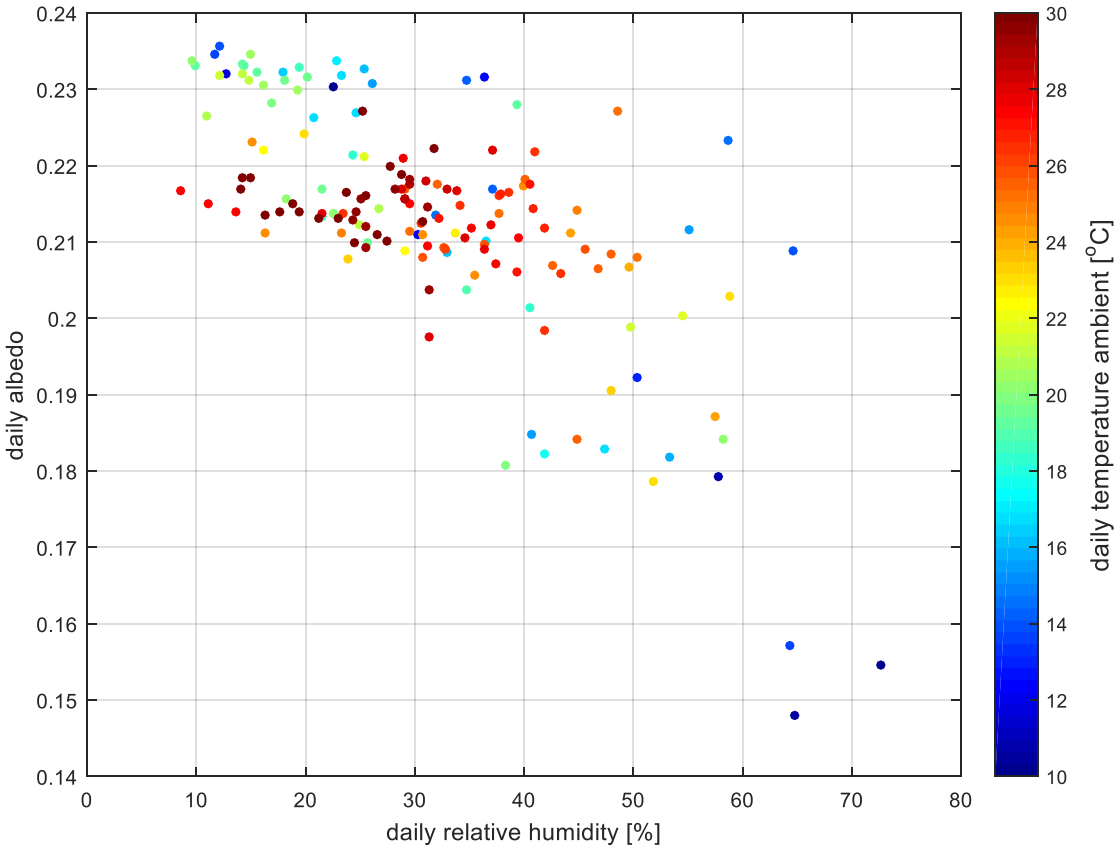


Figure 8: Daytime average albedo plotted as a function of daytime averaged relative humidity, with colors indicating daytime average temperature.

Table I: Temperature and relative humidity (RH) dependent statistics of daytime albedo.

daytime average temperature <25°C	number of days	80
	corr(*albedo*,RH)	-0.8008
	best fit line	$albedo = -0.0009921 * RH + 0.2447$
	R^2	0.6413
daytime average temperature >25°C	number of days	80
	mean daily albedo	0.2133
	max daily albedo	0.2271
	min daily albedo	0.1841
	standard deviation of daily albedo	0.006139
	% of daily albedos between 0.21 and 0.22	67.5%

To further compare different albedos, Figure 9 shows spectral plots collected every 5 minutes from 9AM to 3PM on clear day April 19th and cloudy day May 16th. Normalized spectral plots (normalized to the maximum intensity) are also shown in Figure 9 to allow for easier comparison between different time intervals. Additionally, all spectral plots are color coded based on the albedo measured at that time by the albedometer.

On April 29th (a clear day), all spectra during the 9AM to 3PM time period were very similar, and there was little variation in albedo. On May 16th (a partly cloudy day), however, significant variation is seen in both spectral intensity and albedo. There is no clear pattern between spectral intensity and albedo: low albedo values are observed for spectra with both large and small integrals (corresponding to high and low irradiances). However, after normalization it becomes clear that low albedo corresponds with a shift in spectrum towards shorter wavelengths (the blue end of the spectrum).Times with low albedo had higher relative intensities in the 500-800 nm band and lower relative intensities in the 900-1700 nm band.

It is likely that this shift to shorter wavelengths combined with the ground surface having less reflectance at shorter wavelengths leads to the low albedo. For example, light gray concrete (which may have similar reflective properties as the light grey gravel surrounding the albedometer) has a lower reflectance at wavelengths in the 500-800 nm range than it does in the 900-1700 nm range [15].

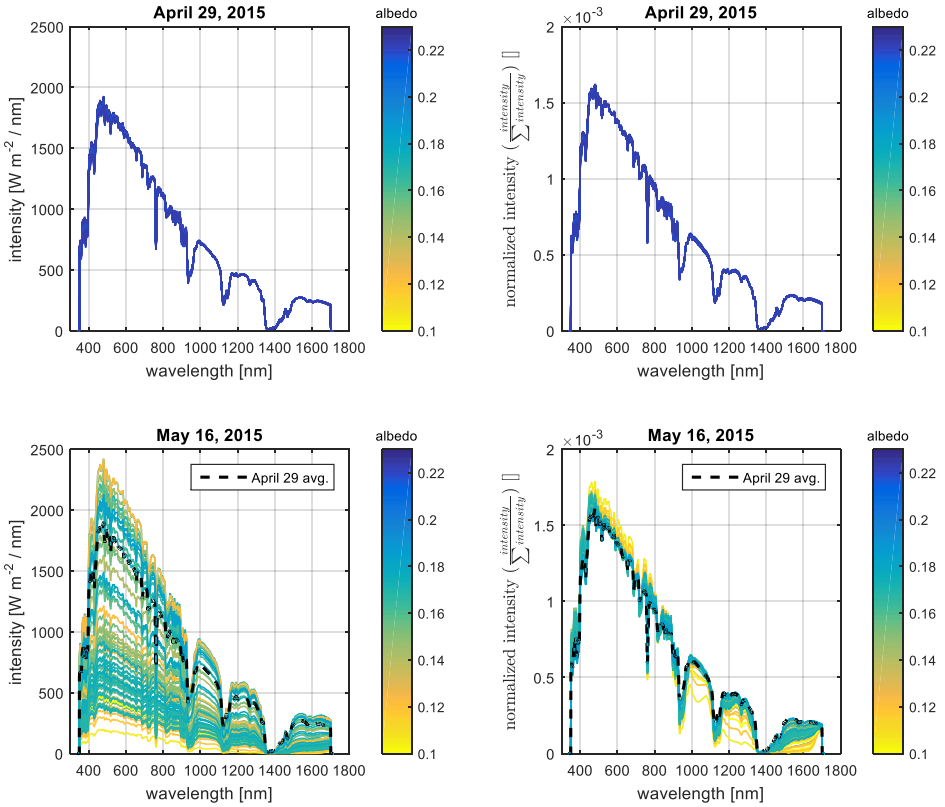


Figure 9: Spectral plots for [top] a clear day (April 29th) and [bottom] a partly cloudy day with low daily average albedo (May 16th). Left plots show absolute intensity, right plots show normalized intensity. The average spectrum for April 29th is included as a dashed black line on the May 16th plots for reference.

4.2. Diffuse Plane of Array (DPOA)

A timeseries plot of the DPOA measurements is shown in Figure 10. The DPOA measurement uses a manually-adjusted shadowband that must be moved every few days. In Figure 10, the period when the shadowband was not properly adjusted (April 15th through April 28th), is highlighted in red. The misalignment of the shadowband resulted in abnormally high measurements, since the sensor was effectively measuring POA rather than DPOA, and so these times are removed from our analysis of DPOA.

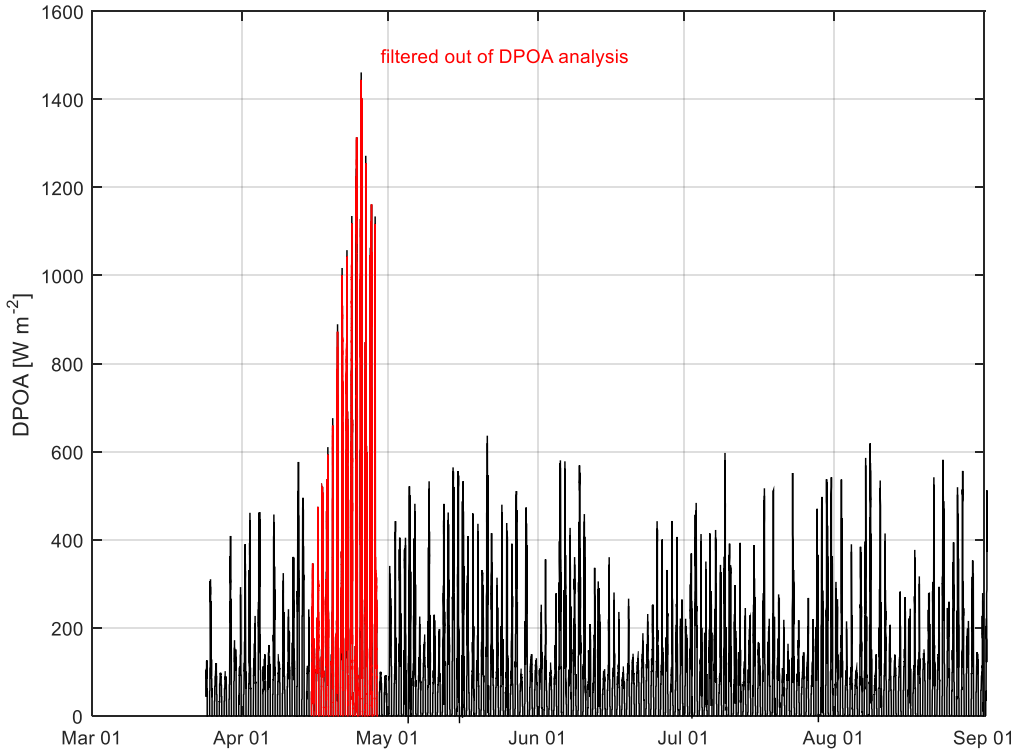


Figure 10: Timeseries of DPOA measurements. The times highlighted in red were filtered out due to the shadowband being misaligned.

The POA and DPOA measurements on the five clear days are shown in Figure 11. Due to seasonal changes in sun angles (as seen in the bottom plot of Figure 11), POA measurements vary systematically on the clear days. POA irradiance is largest in March when angle of incidence at solar noon is smallest. Higher angles of incidence at solar noon in April and August lead to smaller clear day POA measurements. In June when the sun is highest in the sky, the angle of incidence at solar noon is largest and hence the June clear day POA measurement is the smallest of the five clear days.

However, such seasonal behavior is not seen in the DPOA measurements. DPOA values were larger on August 19th than on the other clear days.

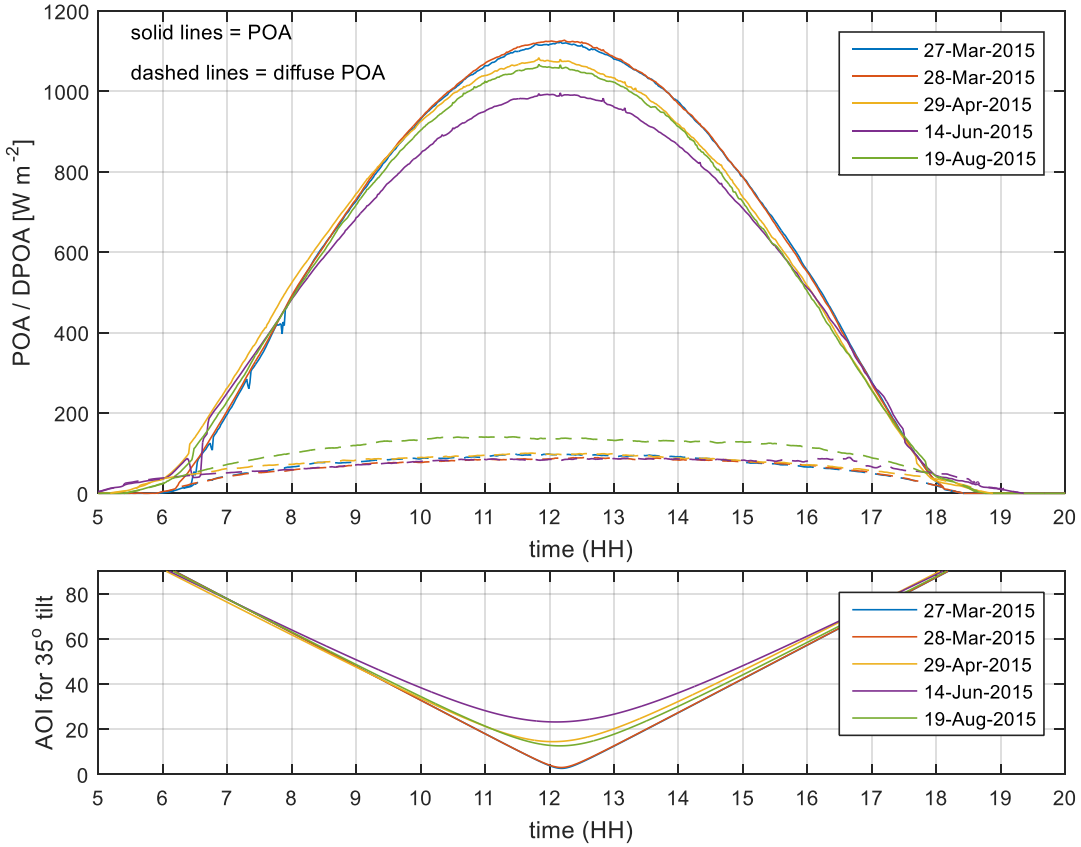


Figure 11: [Top] POA and DPOA on the 5 clear days. [Bottom] Angle of incidence (AOI) for the 35° tilted POA measurement on the 5 clear days.

DPOA can also be calculated from the traditional DNI and POA measurements by subtracting the direct irradiance incident on the plane from the total POA irradiance:

$$DPOA_{calc} = POA - DNI \times \cos(AOI). \quad (12)$$

Figure 12 plots the $DPOA_{calc}$ versus the measured DPOA. The correlation between these two quantities is strong, but there are some discrepancies: a clear trend for $DPOA<DPOA_{calc}$ and negative values of $DPOA_{calc}$ at very low DPOA.

The mean bias difference ($DPOA_{calc}$ - DPOA) is +5.75 Wm^{-2}, meaning $DPOA_{calc}$ is, on average larger than DPOA. This bias seems strongest at large DPOA values (i.e., $DPOA>400$ Wm^{-2}), where $DPOA_{calc}$ was almost always larger than DPOA. From the clear sky days included in Figure 12, we also observe that the relationship between $DPOA_{calc}$ and DPOA is not always the same in the morning versus the afternoon. This is especially clear in the ring-like pattern seen for the August 19th data.

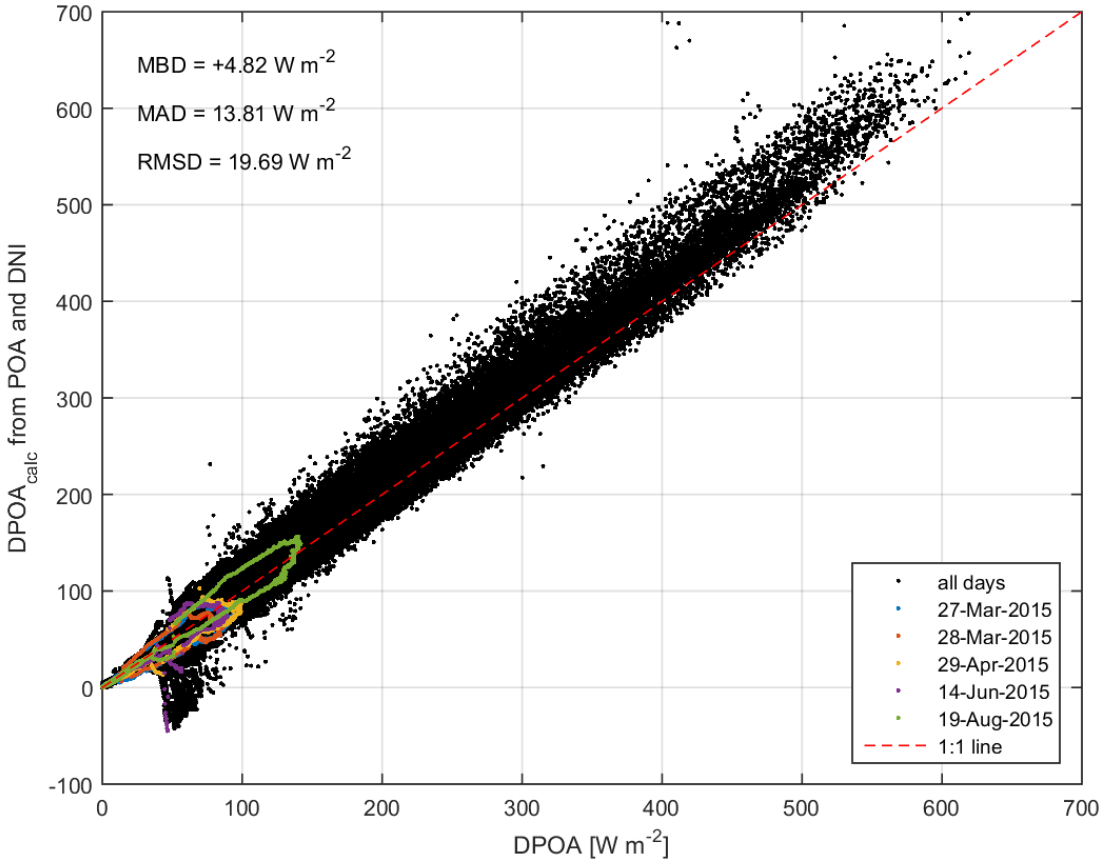


Figure 12: Calculated DPOA (using Equation 12) plotted against measured DPOA. Mean bias difference (MBD), mean absolute difference (MAD), and root mean squared difference (RMSD) statistics describing the difference $DPOA_{calc}$ minus DPOA are shown in the top left.

To further examine these morning versus afternoon discrepancies, Figure 12 shows the measured and calculated DPOA on the five clear days. Also included in Figure 12 is the difference between calculated and measured DPOA. On all of these clear days, the calculated DPOA was larger than the measured DPOA in the morning, and the calculated DPOA was less than the measured DPOA in the afternoon. This may indicate a discrepancy among the azimuths of the DNI, POA, or DPOA measurements.

Figure 14 investigates possible azimuth errors. DNI measurements are found to have, on average, roughly no bias between morning and afternoon measurements. Figure 14 shows DNI morning versus afternoon differences as a function of POA angle of incidence for consistency with other plots; for symmetry analysis (i.e., morning vs. afternoon measurements), equivalent results would be seen if plotted against solar elevation angle or any other angle symmetric around due south. The POA measurements, though, seem to show a bias towards higher morning than afternoon values at the same tilt angles. The smaller plots in Figure 14 show POA morning versus afternoon differences as a function of angle of incidence for various possible POA measurement azimuths. Assuming an azimuth of 178° for the POA instrument shows the least deviation between morning and afternoon measurements, and may be the true azimuth of the POA measurement. This will be considered when testing transposition models.

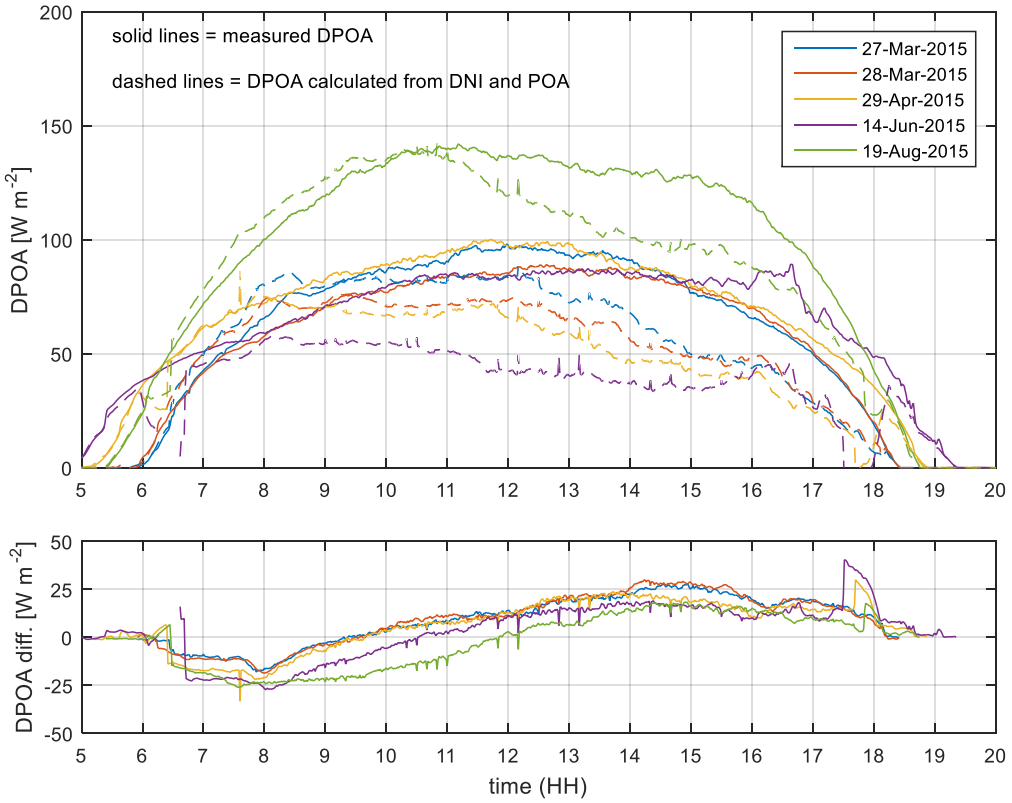


Figure 13: [Top] Measured DPOA and calculated DPOA (using Equation 12). [Bottom] Difference (calculated DPOA minus measured DPOA).

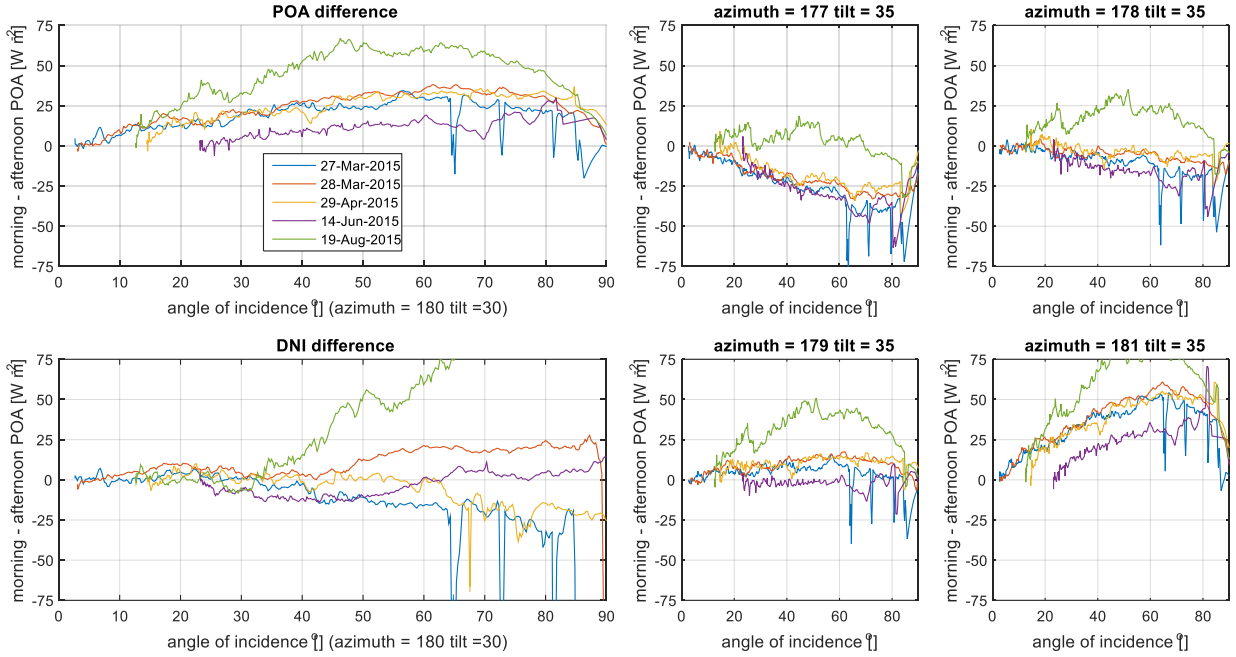


Figure 14: [Top Left] Difference (morning minus afternoon) in POA irradiance, plotted as a function of angle of incidence at a 30° tilt, due south azimuth. [Bottom Left] Same as top left, but for DNI. [Right Plots] Same as top left, but assuming varying azimuths.

Another curiosity in Figure 12 is the negative values obtained for $DPOA_{calc}$. Based on Equation 12, negative $DPOA_{calc}$ values occur when $DNI * cos(AOI) > POA$. In other words, the direct component calculated to be incident on the plane of array is actually greater than the global irradiance (direct plus diffuse) measured on the plane of array.

Most of the negative $DPOA_{calc}$ values result from near-field shading of the POA instruement. Figure 15 plots these negative $DPOA_{calc}$ values as a function of solar azimuth and solar elevation angles. On this plot, it is clear that most of the negative $DPOA_{calc}$ values occur at specific combinations of solar azimuth and elevation: 318 of the 327 total minutes with negative $DPOA_{calc}$ values occur when the solar azimuth is between 73° and 80° (i.e., north of east) and the solar elevation is between 12° and 19°. Large trees and power poles in that direction shade the POA measurement during these times while the DNI measurement remains unshaded. We eliminated these shaded times by applying a filter to remove all POA measurements when the solar azimuth and elevation was within these bounds, as indicated by the blue box in Figure 12. The effect of this filter on the data for June 14th is shown in Figure 16.

The remaining nine negative $DPOA_{calc}$ values not eliminated by the shading filter are small (none less than -1 Wm^{-2}) and likely result from noise in the measurements. All nine values occurred in the early morning or late evening when both DNI and POA measurements were small. These values were manually removed from the analysis since there was not sufficient evidence of systematic shading.

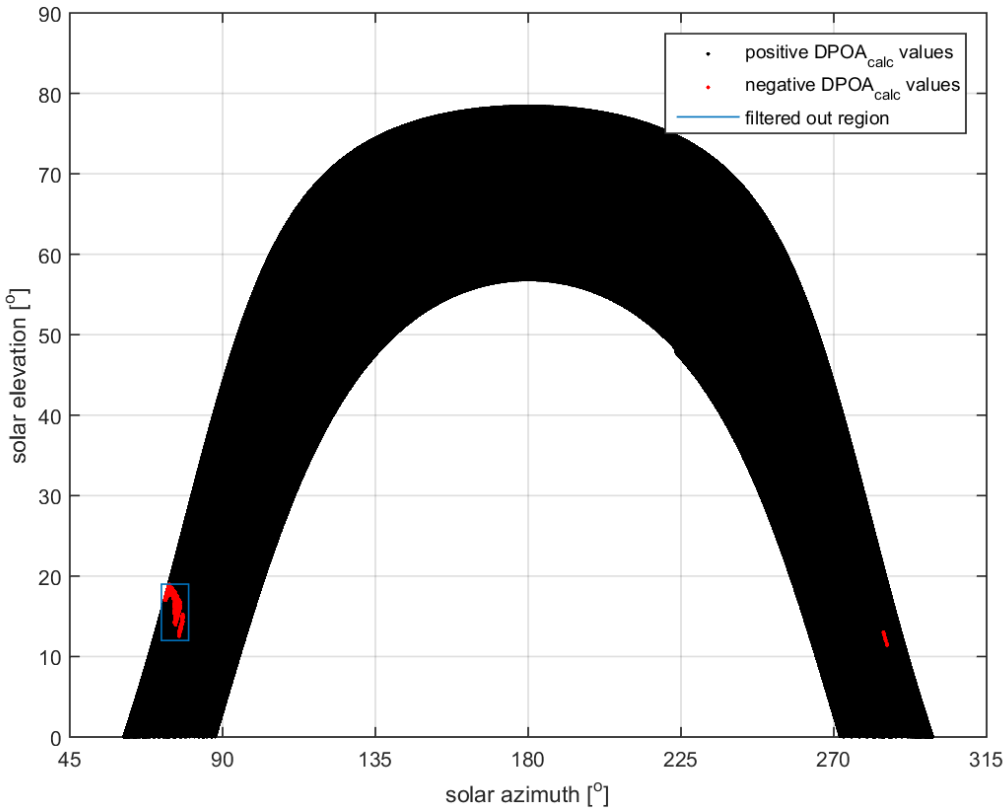


Figure 15: Negative (red) values of $DPOA_{calc}$ as a function of solar azimuth and elevation. The values in the blue box were filtered out of the analysis due to likely shading of the POA sensor.

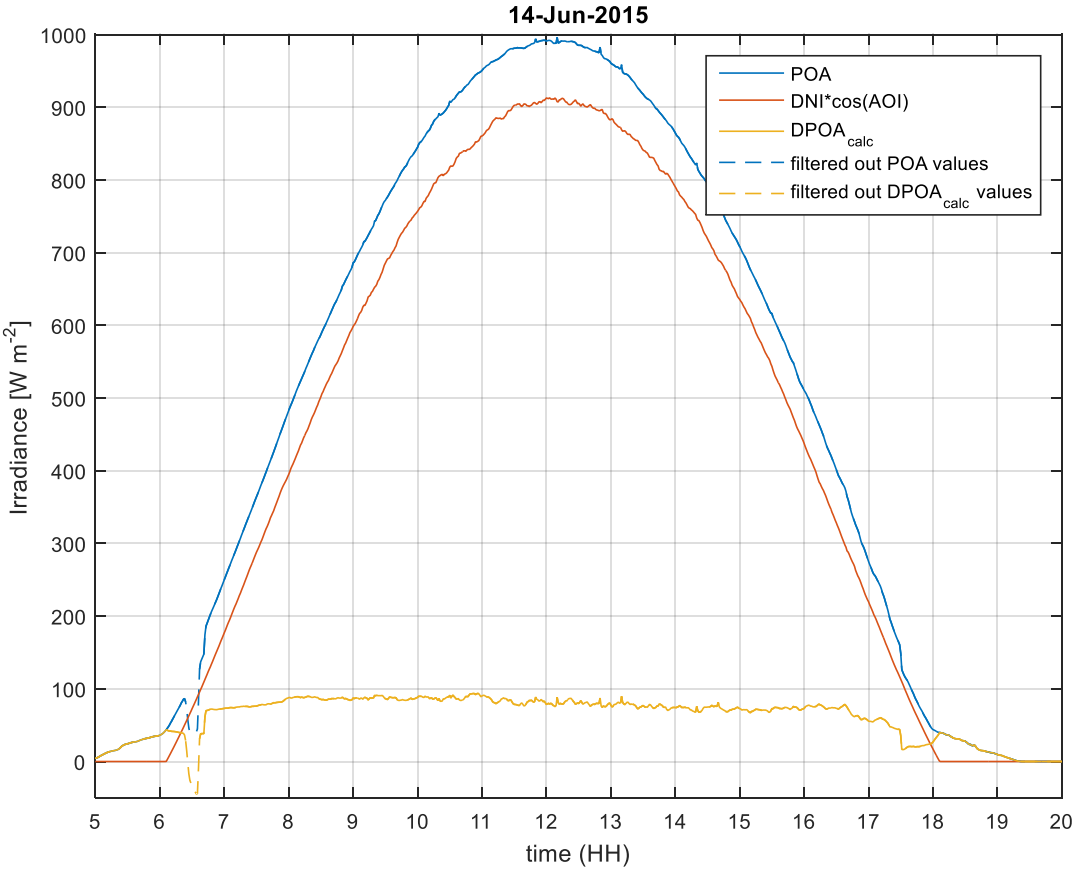


Figure 16: POA, DNI*cos(AOI), and $DPOA_{calc}$ for clear day June 14th. The dashed portions around 06:30 show the effect of filtering out the shaded POA periods seen in Figure 15.

5. EFFECT OF MEASURED ALBEDO ON POA MODELING

The four transposition models listed in section 3 were evaluated. The albedo measurements described in section 4.1 were used to model the ground-reflected diffuse irradiance, and the resulting POA estimates were compared to those obtained when assuming $albedo = 0.2$. Additionally, due to the concerns about measurement uncertainty shown in Figure 3 (redundant GHI measurements deviate by as much as 10 Wm^{-2}), and Figure 14 (POA measurements may not be at a due south azimuth), the results using different combinations of measurements for inputs to transposition models or for POA irradiance are compared.

Inputs to transposition models are typically two of GHI, DHI, and DNI, since the standard equation

$$GHI = DHI + DNI \times \cos(\theta), \tag{13}$$

where θ is the solar zenith angle, can be used to find the third of these quantities if two are specified. Since measurements of GHI (GHI at the weather station was used), DHI, and DNI were available for this study, inputs for transposition models could be derived from GHI and DNI, GHI and DNI, or DHI and DNI. While theoretically all pairs should result in identical inputs, measurement errors will lead to slight discrepancies, and, thus will give an indication of measurement uncertainties.

Similarly, as described in Equation 12, the transposition model output (modeled POA irradiance) can be compared to either the POA measurement or to POA calculated from the DNI and DPOA measurements.

$$POA_{calc} = DPOA + DNI \times \cos(AOI). \tag{14}$$

The 17 minutes when measured POA (either from POA or from DPOA and DNI) minus modeled POA was greater than 200 Wm^{-2} were eliminated from error analysis. Such differences between transposition models are much larger than expected and visual examination determined that these differences are likely due to inappropriate measurement values such as temporary shading of one sensor (e.g., by a person walking past the sensor).

5.1. Modeled versus Measured over Period of Record

Figure 17 shows the mean bias difference (MBD) and root mean squared difference (RMSD) between transposition modeled POA irradiance and measured POA irradiance consisting of either the POA measurement or the POA value calculated from DPOA and DNI. The MBDs are almost all negative. Previous analysis using data from the same instruments over a whole year found transposition biases to be between -1% and +1% for all models except the isotropic model. The larger biases seen here may result from using only a partial year (spring and summer) rather than a full year in this analysis.

Figure 17 also compares transposition model MBD and RMSD for cases with measured albedo (solid lines) and to cases with albedo fixed at $albedo = 0.2$. MBD and RMSD differ by less than 0.15% between corresponding measured and fixed albedo cases. This means that the effect of inaccurate albedo on uncertainty in modeled POA is smaller than the effects from other factors such as differences among transposition models, sensor bias, etc. However, in extreme cases of

very large or very small albedos, the impact of albedo can be significant, as described in Section 5.3.

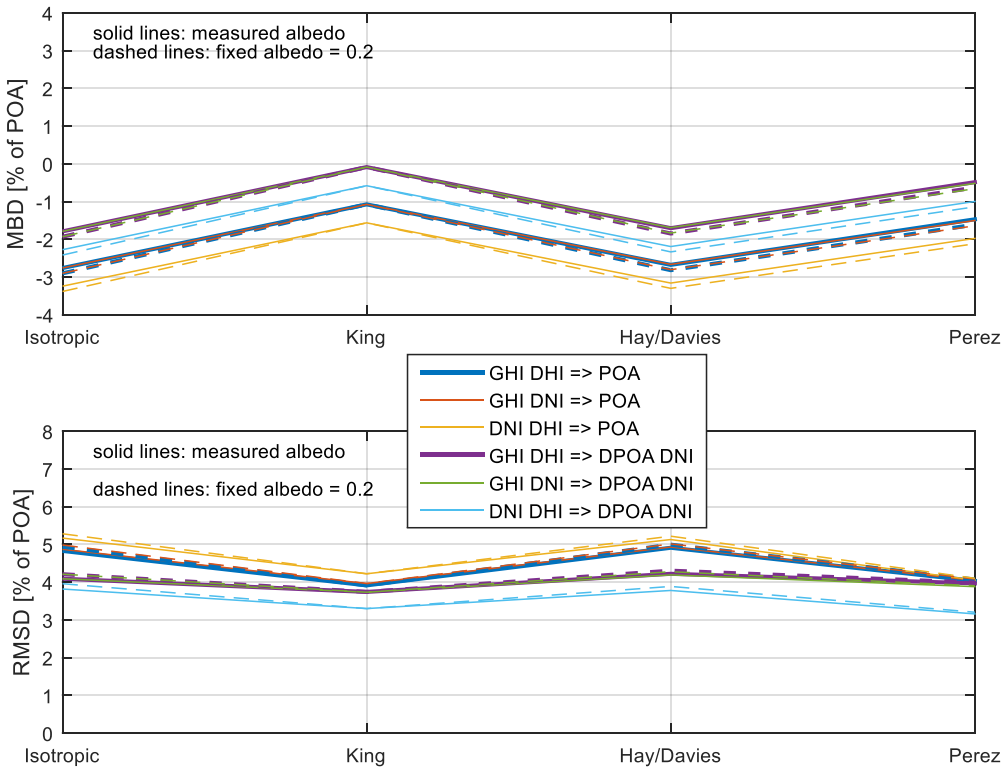


Figure 17: [Top] Mean bias difference and [Bottom] root mean squared difference for combinations of transposition inputs and POA measurements (colors) and for four transposition models (x-axis).

5.2. Time of Day Dependence

To further examine the differences between measured and modeled POA irradiance, Figure 18 shows the mean difference (modeled minus measured) as a function of time of day for each of the four transposition models and six transposition model input and POA measurement combinations. Two trends are apparent in Figure 18. First, all transposition models show negative errors in the morning when compared to the POA instrument measurement. This trend is not seen when the models are compared to the POA calculated from DPOA and DNI. The negative errors have a similar shape and magnitude to the morning negative errors seen in Figure 13, and are likely caused by the same effect (e.g., the POA instrument's azimuth is rotated slightly to the east). Second, it is seen that although the King model had the smallest MBDs (Figure 17), it also has some of the largest variation in within-day modeled minus measured POA. This suggests that the King model is volatile: it appears to work well over a whole day but could result in large errors if used for only part of a day. Future enhancements to the King model should target eliminating this intra-day pattern.

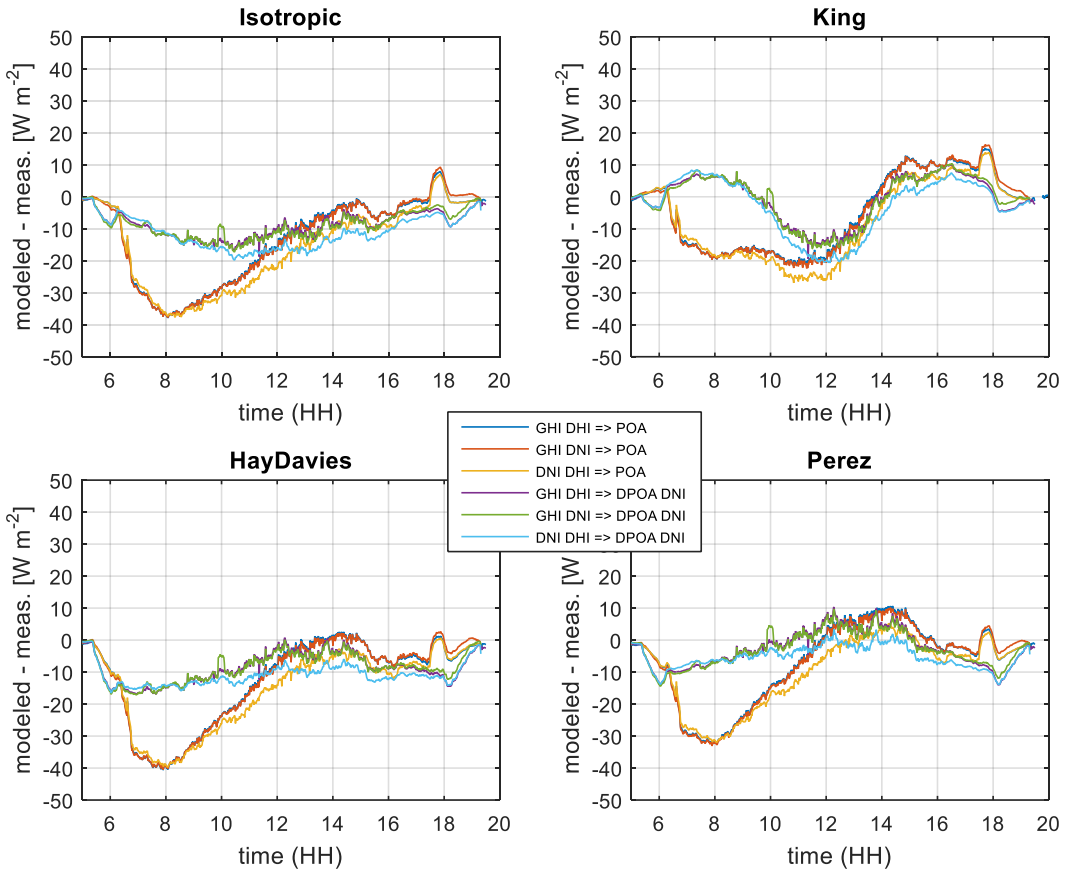


Figure 18: Mean error for each time of day. The different plots [top left, top right, bottom left, bottom right] show the different transposition models, and the various lines (different colors) show the various transposition inputs and POA measurements.

We note that using fixed rather than measured albedo would have little effect on the results in Figure 18: if using fixed $albedo = 0.2$, the mean modeled minus measured values shown in Figure 18 would change by less than 2 Wm^{-2}, which is much smaller than the effect of the two trends identified in the previous paragraph.

5.3. Effect of Assumed Albedo

The results in Figure 14 show very little impact (~0.15% difference in MDB and RMSD) from varying albedo between a fixed albedo $\rho = 0.2$ and the measured albedo, which averaged 0.214. Since all of the data analyzed was from Albuquerque, NM in spring and summer months, there was never snow on the ground which could lead to a drastically larger albedo. Additionally, if the instruments were placed on a black surface rather than the gray gravel, the albedo may have been smaller.

To show the impact that varying albedo can have on transposition MBD and RMSD, in Figure 19 we present results from various fixed albedos. As albedo decreases, the MBD also decreases, and conversely, as the albedo increases the MBD also increases. The King model does not use

albedo as an input (Equation 7), and therefore remains the same regardless of albedo. For the isotropic, Hay/Davies, and Perez transposition models, there is approximately a 1% change in MBD per 0.1 change in albedo. This is equivalent to saying that a 0.1 change in albedo leads to approximately a 1% change in total insolation on the plane of array over the period of record. Because of the surface tilt and GHI dependencies in Equation 5, this change in total insolation will vary based on the plane of array being considered and the total incident GHI: larger tilt angles and larger average GHI values will result in a larger impact from changing albedo.

RMSE is not linear as a function of albedo; rather a minimum in RMSE is seen around $\rho = 0.3$ and $\rho = 0.4$. These values are larger than the measured albedo average of 0.214. We feel it is likely that these larger fixed albedo values are cancelling out errors in the transposition models (seen in Figure 18). Another possibility is that the albedo measurements are errant, but based on the quality of the albedometer instruments, we find this less likely.

Overall, the results shown in Figure 19 demonstrate that deviations from the $\rho = 0.2$ assumption can lead to significant changes in total insolation (and, hence energy production for POA modules). For example, a location with snow on the ground for many days during the year may have an annual average of albedo $\rho = 0.3$, and hence may have approximately 1% more total irradiation than a location with no snow cover.

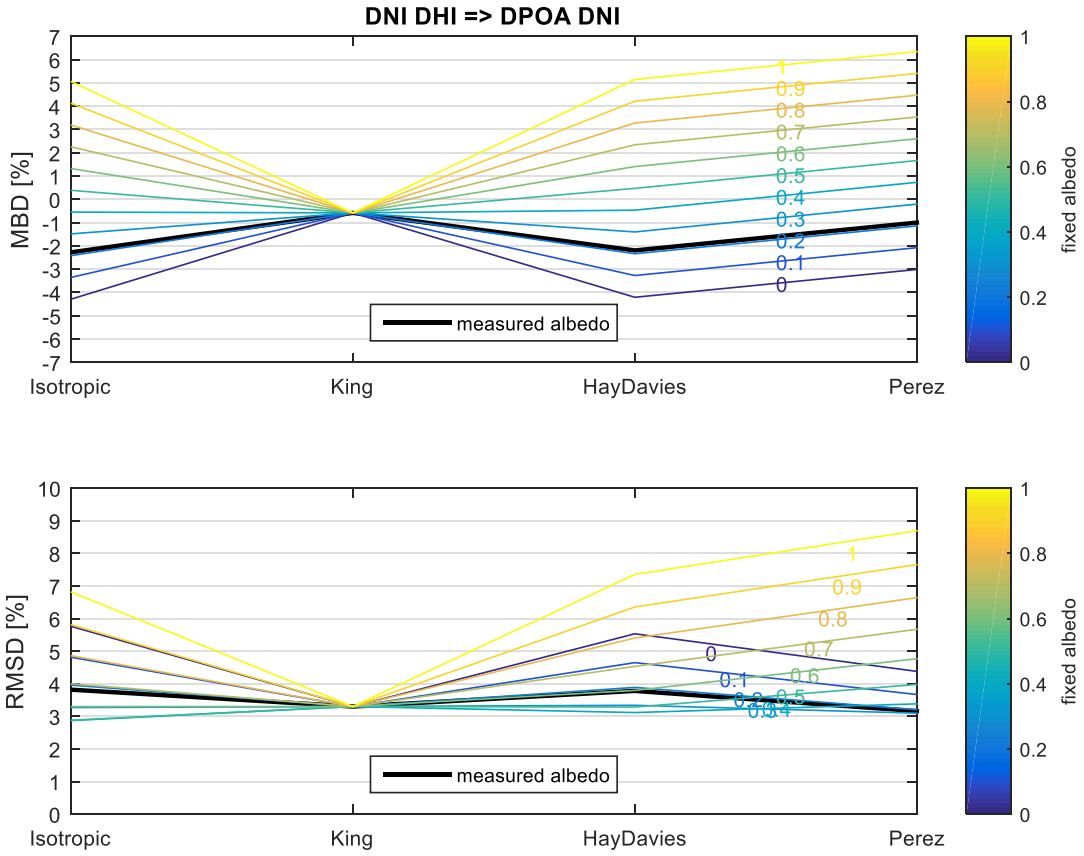


Figure 19: [Top] Mean bias difference and [Bottom] root mean squared difference for different fixed albedo assumptions (colored lines) using four transposition models (x-axis).

5.4. Hourly Analysis

Up to this point, all analysis has been using 1-minute data. However, the transposition models tested were developed and are most often used with hourly data. To compare to the 1-minute results, in this section we recreate Figures 17 and 18 using hourly averages of the data.

Figure 20 shows the MBD and RMSD computed using hourly data. MBDs are nearly identical to those computed with minute data shown in Figure 17. This is expected since time averaging should have little impact on bias [3]. The RMSDs for the combinations which compare modeled POA to POA calculated from DPOA and DNI are reduced by nearly 1% when using hourly data versus minute data. This reduction is due to smoothing of the irradiance during partly cloudy periods that occurs when temporally averaging over an hour, and may also be due to slight offsets in cloud arrival times between the various instruments. However, the RMSDs for the combinations which compare modeled POA to measured POA are nearly the same whether minute or hourly averaged data are used. This may again suggest a bias in the POA measurement (e.g., an azimuth offset) that is not negated by temporal averaging.

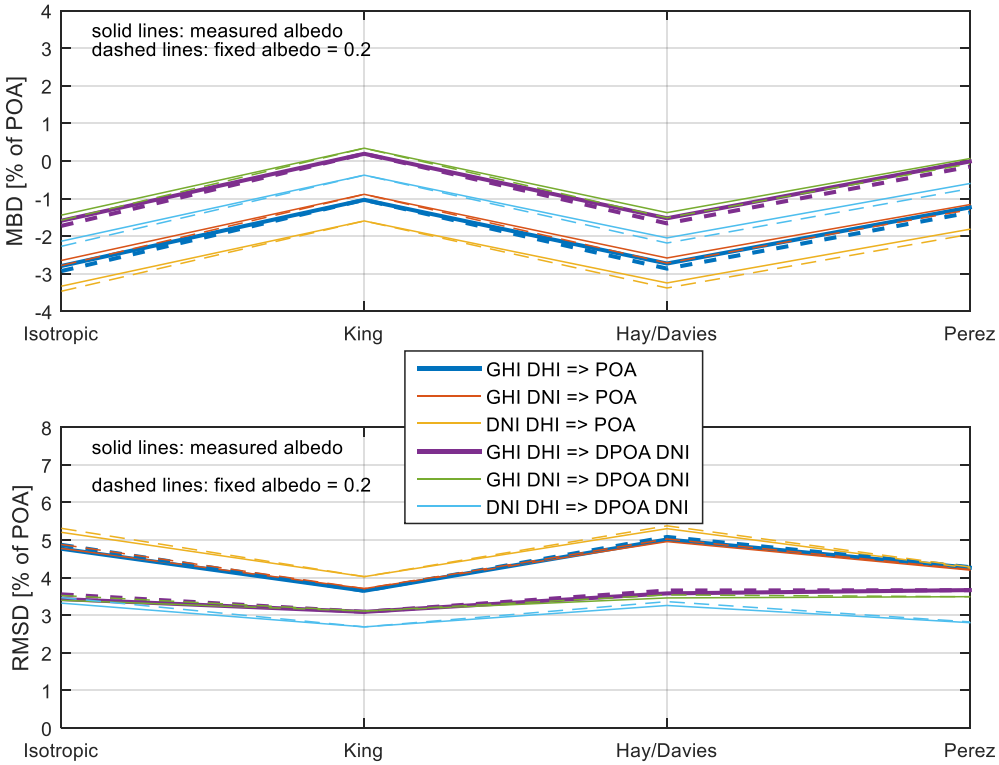


Figure 20: Same as Figure 17, but computed using hourly data.

Figure 21 shows the mean error for each time of day, computed using hourly data. The lines in Figure 21 are smoother than those created using minute data in Figure 18, but otherwise exhibit the same trends: all models have negative errors (underestimate) in the morning when compared to the POA measurement, and the King model shows significant intra-day variation.

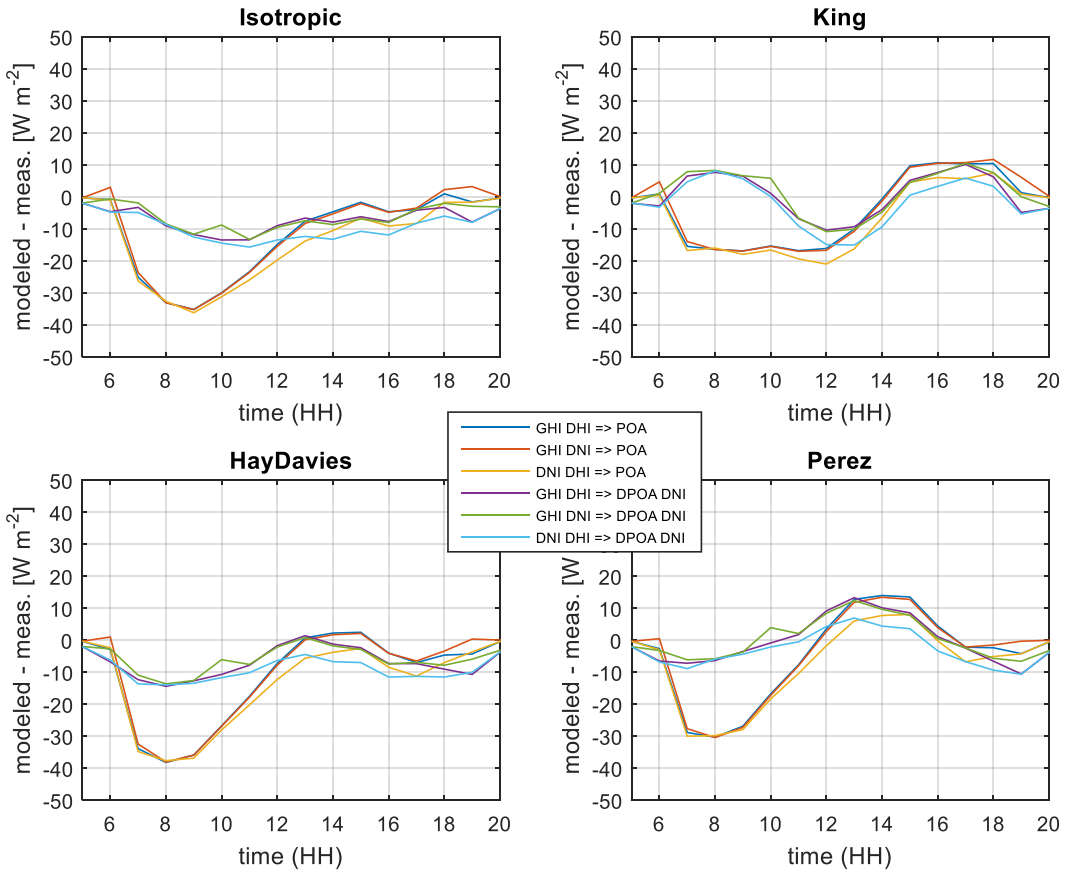


Figure 21: Same as Figure 18, but computed using hourly data..

6. CONCLUSIONS

This work used albedo and diffuse plane of array (DPOA) measurements in addition to more standard global horizontal irradiance (GHI), direct normal irradiance (DNI), diffuse horizontal irradiance (DNI), and plane of array irradiance (POA) measurements to determine the impact of albedo on transposition model performance.

Albedo measurements allowed for analysis of daily albedo and albedo trends. Albedo values at the test site in Albuquerque, NM were typically between 0.2 and 0.25, slightly larger than the common 0.2 assumption. Daily average albedo values did not appear to show seasonal trends, though they did appear to be related to relative humidity. Larger relative humidity values led to smaller daily albedo values.

DPOA measurements allowed for comparison of calculated DPOA values (from POA and DNI) to measured DPOA values. A within-day difference was observed, and it is thus suspected that the POA instrument is not at due south azimuth. This shows the value to having interrelated measurements: without the DPOA measurement, it would have been much more difficult to identify errors in the POA measurement. For example, without the DPOA measurements it would have been difficult or impossible to differentiate an azimuth offset from changes in atmospheric conditions (e.g., increased water vapor in the afternoons could lead to decreased POA irradiance similar to the decrease caused by an azimuth offset).

When using measured albedo (averaging 0.214) versus fixed albedo of 0.2 in transposition models, little difference was seen – only about a 0.15% difference was seen in mean bias difference (MBD) and root mean squared difference (RMSD). Analysis at other fixed albedos showed that increasing albedo by 0.1 is found to increase total modeled insolation (and thus increase MBD) by approximately 1% for the irradiance time series and surface tilt studied. Thus, types of ground cover that are different from the gray gravel surrounding the albedometer in this study (e.g., persistent snow cover, black surfaces, etc.) could lead to significant (i.e., >1%) changes in MBD compared to the 0.2 albedo assumption.

While replacing measured albedo with fixed $albedo = 0.2$ was found to have a small impact for the location studied, measurement deviations had a larger impact. Up to 2% differences in MBD and RMSD were observed when switching between interrelated measurements. For example, when DNI and DHI were used as inputs to the transposition models, and the transposition model output was compared to the POA measurement, the largest magnitude MBDs resulted. When using GHI and DNI as inputs and comparing to POA calculated from DPOA and DNI measurements, the MBDs were about 2% more positive, resulting in the lowest magnitude MBDs.

Based on this analysis, it is recommended that, except in extreme cases of very high or very low albedo (e.g., due to persistent snow cover or black ground covering), plane of array irradiance modeling effort be directed towards quality controlling irradiance measurements and selecting a well-performing transposition model rather than collecting albedo measurements.

REFERENCES

[1] D. G. Erbs, S. A. Klein, and J. A. Duffie, "Estimation of the diffuse radiation fraction for hourly, daily and monthly-average global radiation," *Solar Energy,* vol. 28, pp. 293-302, 1982.

[2] P. Ineichen, R. R. Perez, R. D. Seal, E. L. Maxwell, and A. Zalenka, "Dynamic global-to-direct irradiance conversion models," *ASHRAE Transactions,* vol. 98, pp. 354-369, 1992.

[3] C. A. Gueymard, "Direct and indirect uncertainties in the prediction of tilted irradiance for solar engineering applications," *Solar Energy,* vol. 83, pp. 432-444, 2009.

[4] M. Lave, W. Hayes, A. Pohl, and C. W. Hansen, "Evaluation of Global Horizontal Irradiance to Plane-of-Array Irradiance Models at Locations Across the United States," *Photovoltaics, IEEE Journal of,* vol. 5, pp. 597-606, 2015.

[5] P. G. Loutzenhiser, H. Manz, C. Felsmann, P. A. Strachan, T. Frank, and G. M. Maxwell, "Empirical validation of models to compute solar irradiance on inclined surfaces for building energy simulation," *Solar Energy,* vol. 81, pp. 254-267, 2007.

[6] D. WŁOdarczyk and H. Nowak, "Statistical analysis of solar radiation models onto inclined planes for climatic conditions of Lower Silesia in Poland," *Archives of Civil and Mechanical Engineering,* vol. 9, pp. 127-144, 2009.

[7] Kipp & Zonen. (2004). *Instruction Manual, CM 121 Shadow Ring*. http://www.kippzonen.com/Download/46/CM-121-B-C-Shadow-Ring-Manual

[8] D. King. *Simple Sandia Sky Diffuse Model*. http://pvpmc.org/modeling-steps/incident-irradiance/plane-of-array-poa-irradiance/calculating-poa-irradiance/poa-sky-diffuse/simple-sandia-sky-diffuse-model/

[9] B. Y. H. Liu and R. C. Jordan, "The long-term average performance of flat-plate solar-energy collectors: With design data for the U.S., its outlying possessions and Canada," *Solar Energy,* vol. 7, pp. 53-74, 1963.

[10] J. Torres and L. Torres, "Angular Distribution of Sky Diffuse Radiance and Luminance," in *Modeling Solar Radiation at the Earth's Surface*, V. Badescu, Ed., ed: Springer Berlin Heidelberg, 2008, pp. 427-448.

[11] B. Y. H. Liu and R. C. Jordan, "The interrelationship and characteristic distribution of direct, diffuse and total solar radiation," *Solar Energy,* vol. 4, pp. 1-19, 1960.

[12] J. E. Hay and J. A. Davies, "Calculations of the solar radiation incident on an inclined surface," in *Proc. of First Canadian Solar Radiation Data Workshop, 59*, 1980.

[13] R. Perez, R. Seals, P. Ineichen, R. Stewart, and D. Menicucci, "A new simplified version of the perez diffuse irradiance model for tilted surfaces," *Solar Energy,* vol. 39, pp. 221-231, 1987.

[14] Kipp & Zonen. (2013). *Instruction Manual, CMP Series Pyranometer*. http://www.kippzonen.com/Download/72/Manual-Pyranometers-CMP-series-English

[15] USGS. (2006). *Digital Spectral Library 06*. http://speclab.cr.usgs.gov/spectral.lib06/ds231/PLOTS/A/concrete_gds375.27862.w1.gif

DISTRIBUTION

1	MS0899	Technical Library	9536 (electronic copy)


Sandia National Laboratories